Red, Yellow, Green, and Blue Amplified Spontaneous Emission and Lasing Using Colloidal CdSe Nanoplatelets

Chunxing She,[†] Igor Fedin,[†] Dmitriy S. Dolzhnikov,[†] Peter D. Dahlberg,[∥] Gregory S. Engel,[†,⊥] Richard D. Schaller,[‡,§] and Dmitri V. Talapin*[,†,‡]

[†]Department of Chemistry and the James Franck Institute, University of Chicago, Chicago, Illinois 60637, United States, [‡]Center for Nanoscale Materials, Argonne National Laboratory, Argonne, Illinois 60439, United States, [§]Department of Chemistry, Northwestern University, Evanston, Illinois 60208, United States, [∥]Graduate Program in the Biophysical Sciences, the James Franck Institute, and The Institute for Biophysical Dynamics, University of Chicago, Chicago, Illinois 60637, United States, and [⊥]The Institute for Biophysical Dynamics, University of Chicago, Chicago, Illinois 60637, United States

ABSTRACT There have been multiple demonstrations of amplified spontaneous emission (ASE) and lasing using colloidal semiconductor nanocrystals. However, it has been proven difficult to achieve low thresholds suitable for practical use of nanocrystals as gain media. Low-threshold blue ASE and lasing from nanocrystals is an even more challenging task. Here, we show that colloidal nanoplatelets (NPLs) with electronic structure of quantum wells can produce ASE in the red, yellow, green, and blue regions of the visible spectrum with low thresholds and high gains. In particular, for blue-emitting NPLs, the ASE threshold is 50 μJ/cm^2, lower than any reported value for nanocrystals. We then demonstrate red, yellow, green, and blue lasing using NPLs with different thicknesses. We find that the lateral size of NPLs does not show any strong effect on the Auger recombination rates and, correspondingly, on the ASE threshold or gain saturation. This observation highlights the qualitative difference of multiexciton dynamics in CdSe NPLs and other quantum-confined CdSe materials, such as quantum dots and rods. Our measurements of the gain bandwidth and gain lifetime further support the prospects of colloidal NPLs as solution-processed optical gain materials.

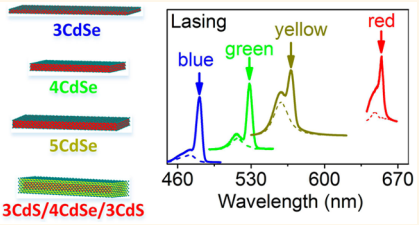

KEYWORDS: nanoplatelets · semiconductor nanocrystals · Auger recombination · optical gain · amplified spontaneous emission · lasing

Highly luminescent colloidal semiconductor nanocrystals[1] have been widely explored as optical gain media[2−10] because of their tunable emission and gain wavelengths, low cost, and solution processability. The early demonstrations of optical gain and lasing using colloidal quantum dots (QDs) showed that high pump thresholds, typically on the order of 1 mJ/cm^2, were required to generate amplified spontaneous emission (ASE).[2−10] These high thresholds retarded the demonstration of multicolor lasing using QDs, particularly in the blue. The major obstacle is fast nonradiative Auger recombination,[11] which causes the fast decay of the biexciton state required for optical gain. Various shapes and compositions of nanocrystals, for example, spherical "giant" QDs,[12] quantum rods (QRs),[5,9] and tetrapods,[13] have been designed to reduce Auger recombination rates. Alternatively, nanocrystals supporting the single-exciton gain mechanism,[8,14,15] which bypasses losses through Auger recombination, have also been proposed to reduce the threshold. These efforts have pushed the threshold down to sub-100 μJ/cm^2,[12,13,15] and multicolor lasing using QDs was further demonstrated.[15] Using colloidal nanoplatelets (NPLs), with the electronic structure of quantum wells,[16] our recent work showed a record low ASE threshold of 6 μJ/cm^2.[17] Green lasing using these NPLs thus became possible.[18] Moreover, the low threshold renders continuous-wave lasing feasible,[19] which opens up opportunities for pumping NPL lasers with GaN LEDs and other inexpensive light sources.

ASE and lasing in the blue range are particularly challenging because blue emission typically requires small nanocrystals, in which the Auger rate increases inversely with the nanocrystal volume.[11] In addition, small QDs have high surface-to-volume ratios that can lead to a high density of trap states.

* Address correspondence to dvtalapin@uchicago.edu.

Received for review April 27, 2015 and accepted August 21, 2015.

Published online August 24, 2015
10.1021/acsnano.5b02509

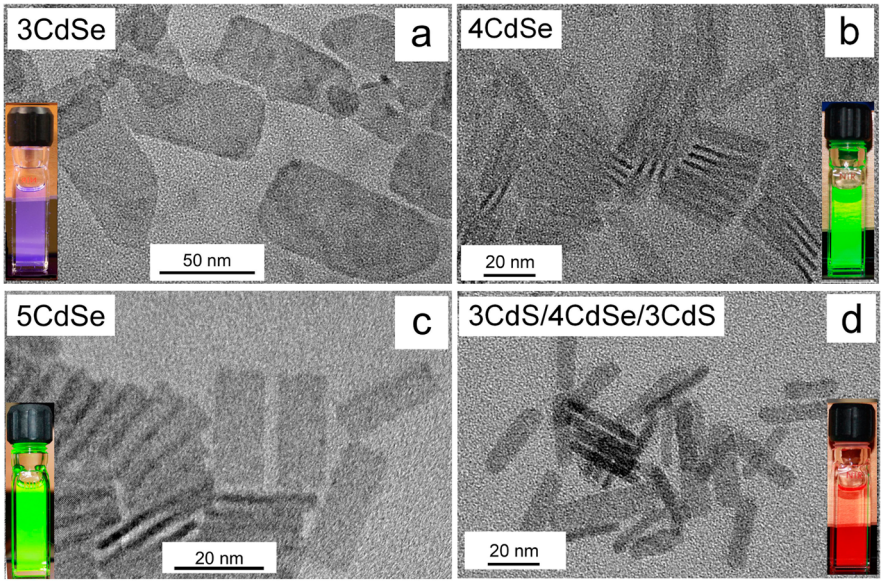

Figure 1. Transmission electron microscope images of (a) 3CdSe, (b) 4CdSe, (c) 5CdSe, and (d) 3CdS/4CdSe/3CdS NPLs. Insets are luminescence photographs of clear NPL colloidal solutions.

Blue ASE was initially observed at liquid nitrogen temperature,[7] although blue lasing was achieved at room temperature shortly after, with a threshold of 3.7 mJ/cm^2.[20] By carefully engineering core/shell alloyed QDs,[15,21] Auger recombination rates were partially suppressed potentially due to a smooth confinement potential,[22] and the ASE threshold was further reduced to 60 μJ/cm^2.[21] However, blue lasing from these systems has not been demonstrated.

While the ASE threshold determines the lowest energy input for lasing, the gain saturation limits the maximum optical output power. An ideal lasing medium should exhibit a high dynamic range, with low ASE threshold and high threshold for gain saturation. The gain saturation in QD lasing is expected to occur at fluences of just twice the ASE threshold.[12,23] In contrast, gain saturation in NPLs occurs at fluences over 2 orders of magnitude higher than the ASE threshold.[17] Understanding factors affecting gain saturation in NPLs can provide clues to designing even better lasing media.

Here, we expand the ASE measurements to red-, yellow-, green-, and blue-emitting NPLs, and we show that all these NPLs produce ASE with low thresholds. We observed thresholds of 50 μJ/cm^2 for blue ASE, 17 μJ/cm^2 for green ASE, 28 μJ/cm^2 for yellow ASE, and 6 μJ/cm^2 for red ASE, all from NPLs with different thicknesses. In particular, the threshold for blue-emitting NPLs is one of the lowest reported values for blue-emitting nanocrystals. We also measured the NPL's modal gain, reaching 690 cm^{-1}, which is a several-fold increase compared to the largest values reported for colloidal quantum dots and rods. We further demonstrate red, yellow, green, and blue lasing by placing these NPLs in simple optical cavities. We measure the gain bandwidth and gain lifetime of red-emitting NPLs to provide more insights into their superior performance. The gain bandwidth of red-emitting NPLs is about 0.22 eV, and their gain lifetime is 140 ps, which is longer than that of QDs. Moreover, we tuned the lateral dimensions of NPLs to examine the effect on the ASE threshold and gain saturation. We find only a weak effect of lateral dimensions on NPL gain properties. However, a significantly higher gain saturation threshold is observed in NPLs emitting at 550 nm compared to those emitting at 512 nm. We explain these effects using measured multiexciton recombination rates.

RESULTS AND DISCUSSION

Synthesis and Structural Characterization of Colloidal CdSe NPLs. We synthesized CdSe NPLs with different thicknesses. The thickness is characterized by *x* monolayers of CdSe with corresponding numbers of Se layers as required by the symmetry of a zinc blend crystal lattice, which we term *x*CdSe. All CdSe NPLs were synthesized by solution-phase colloidal synthesis following previously published procedures[24] with slight modifications. Different combinations of Cd and Se precursors were used to synthesize 3CdSe, 4CdSe, and 5CdSe NPLs at different temperatures and precursor introduction sequences (see Methods for details). Moreover, by growing CdS shells on the top and bottom surfaces of the CdSe NPL using the colloidal atomic layer deposition technique,[25] shell/core/shell NPLs were also synthesized, and they are termed *x*CdS/*y*CdSe/*x*CdS, where *x* and *y* are the thicknesses measured in monolayers. Figure 1 shows transmission electron microscope (TEM) images of 3CdSe, 4CdSe, 5CdSe, and 3CdS/4CdSe/3CdS NPLs. The thicknesses of these NPLs

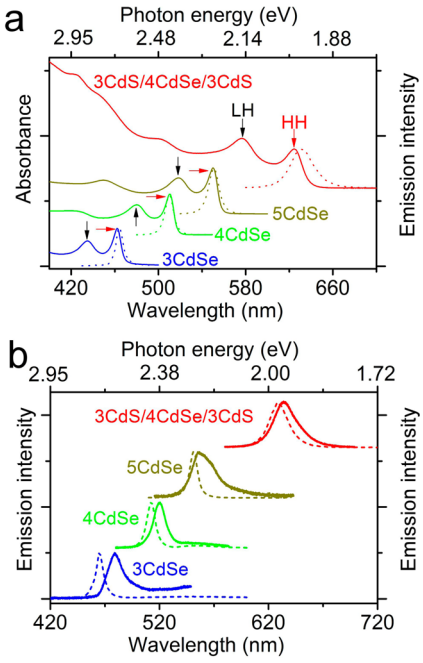

Figure 2. (a) Absorption (solid lines) and emission (dashed lines) spectra of NPLs emitting at 462 nm (3CdSe), 512 nm (4CdSe), 550 nm (5CdSe), and 630 nm (3CdS/4CdSe/3CdS) in hexane solutions. The black and red arrows indicate the excitonic transitions that involve light holes (LH) and heavy holes (HH), respectively. (b) Emission spectra of 3CdSe, 4CdSe, 5CdSe, and 3CdS/4CdSe/3CdS NPLs in hexane (dash lines) and in films (solid lines). The excitation wavelength is 400 nm.

are 0.9, 1.2, 1.5, and 3.0 nm, respectively. The lateral dimensions differ significantly: 60 ± 5 nm by 40 ± 7 nm for 3CdSe, 27 ± 3 nm by 7 ± 2 nm for 4CdSe, 25 ± 3 nm by 10 ± 1 nm for 5CdSe, and 28 ± 3 nm by 8 ± 2 nm for 3CdS/4CdSe/3CdS. They form stable, clear colloidal solutions (see luminescence photographs in Figure 1).[16,26]

Absorption and Emission Spectroscopy. The NPL emissions transit from blue (3CdSe) to green (4CdSe and 5CdSe) and further to the red for core/shell NPLs (3CdS/4CdSe/3CdS).[25] The emission quantum yields of these NPLs are generally high; for example, it is around 50% for 5CdSe,[16,27] and it can reach 80% for the core/shell NPLs.[28,29] Figure 2 shows the absorption and emission spectra of NPLs in hexane emitting at 462 nm (3CdSe), 512 nm (4CdSe), 550 nm (5CdSe), and 630 nm (3CdS/4CdSe/3CdS). Excitonic transitions involving light hole (LH) and heavy hole (HH) states are readily observed in each absorption spectrum, consistent with theoretical predictions.[16] For example, the peaks are located at 577 nm (LH) and 625 nm (HH) for 3CdS/4CdSe/3CdS. Compared with the quantum-confined LH and HH transitions, the absorption of *x*CdSe NPLs is relatively weak in the blue spectral region (<420 nm). On the contrary, 3CdS/4CdSe/3CdS NPLs absorb much stronger in the blue region. This stronger absorption, combined with the red-shift of LH and HH transitions, clearly indicates growth of CdS shells on the CdSe NPL because electron wave functions in the CdSe NPL extend into the CdS layers. These CdS shells significantly increase the absorption cross sections in the blue region.[17]

Unlike any colloidal QD samples, NPL samples effectively eliminate inhomogeneous broadening of absorption and emission spectra by exploiting atomically precise, identical thicknesses. Measurements of photoluminescence excitation (PLE) spectra support this claim (Figure S1). As a result, the emission (and the lowest energy absorption) spectra of all these CdSe NPLs are narrow (fwhm <40 meV)[16,27,29] and typically of Lorentzian shape.[16] The line width becomes slightly broader after growing the CdS shells on the CdSe cores (3CdS/4CdSe/3CdS), likely due to increased electron–phonon coupling.[29] Similar to *x*CdSe NPLs, the core–shell NPLs do not show inhomogeneous broadening.[17,25]

The NPLs form densely packed and optically transparent films when spin coated on glass. The refractive indices determined using ellipsometry are 1.9 ± 0.2, 1.7 ± 0.2, 1.9 ± 0.2, and 1.9 ± 0.1, for 3CdSe, 4CdSe, 5CdSe, and 3CdS/4CdSe/3CdS NPLs, respectively. We estimated the volume fraction of CdSe (or CdSe/CdS) in films using the equation $D = (n_{film} - n)/(n_{CdSe} - n)$, where D is the semiconductor volume fraction, n_{film} is the film refractive index, and n is the refractive index of either ligands or air ($n_{ligands} = 1.46$, $n_{air} = 1$, $n_{CdSe} = 2.4$), and we calculated the semiconductor volume fraction to be in the range of 47% to 64% for 3CdSe, of 26% to 50% for 4CdSe, of 47% to 64% for 5CdSe, and of 47% to 64% for 3CdS/4CdSe/3CdS. Because the refractive indices of the NPL films are greater than that of glass, these films serve as waveguides guiding emission to the film edges.

Weak trap emission bands are often noticeable for *x*CdSe NPLs in solutions, particularly for 3CdSe (Figures 2b and S2a).[24] PLE spectrum measurements clearly indicate that these emissions originate from trap states in the NPLs rather than an impurity (Figure S2b). The trap emissions appear more pronounced in NPL films (Figure 2b), presumably due to energy transfer, which can occur very efficiently between stacked NPLs,[30] from nondefective to defective NPLs,[31,32] and due to self-absorption that reduces the band-edge emission (the photon energies of trap emissions are too low to be reabsorbed).[33]

Amplified Spontaneous Emission. ASE is observed by exciting these optically uniform films at 400 nm using femtosecond pulses and monitoring emissions from the film edge. Figure 3a shows the typical pump-fluence-dependent ASE spectra from films of 3CdSe, 4CdSe, 5CdSe, and 3CdS/4CdSe/3CdS NPLs. Spontaneous emission is observed at low pump fluences, while a sharp ASE peak appears on the red shoulder of the emission band at higher pump fluences. The plots of pump-fluence-dependent total emission intensities indicate ASE thresholds, above which the intensity increases with a steeper slope (Figure 3b). Representative ASE

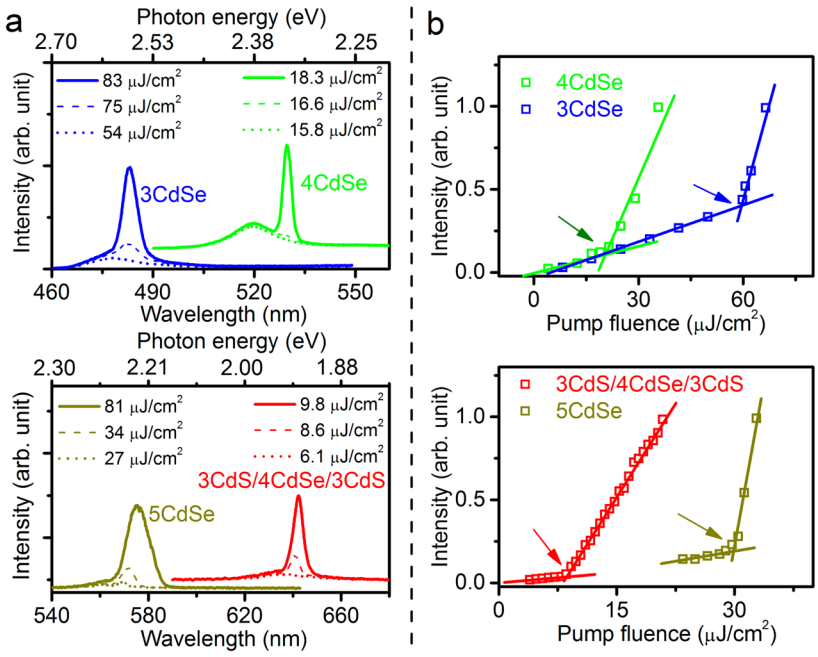

Figure 3. (a) Spontaneous emission (dotted lines) and amplified spontaneous emission (ASE, solid lines) spectra of films of 3CdSe, 4CdSe, 5CdSe, and 3CdS/4CdSe/3CdS NPLs. ASE peaks appear on the red shoulder of spontaneous emission bands at higher pump fluences. Samples were excited at 400 nm using femtosecond pulses. (b) Pump-fluence-dependent total emission intensity. Dots are experimental data. Solid lines are linear fits to the data in different regions. The arrows point to ASE thresholds.

spectra and thresholds are shown in Figure 3. After measuring over 10 films for NPLs with each thickness, we obtained a distribution of thresholds[17] that is likely due to variations of film microstructure. The lowest thresholds are 50, 17, 28, and 6 μJ/cm^2 for 3CdSe, 4CdSe, 5CdSe, and 3CdS/4CdSe/3CdS NPLs, respectively. These thresholds are lower than the best results for carefully engineered QDs emitting at the same spectral range.[12,15] Unfortunately, the distribution of ASE threshold renders accurate comparison among different NPLs difficult at this point.

The threshold for the blue-emitting 3CdSe NPLs is particularly impressive: 50 μJ/cm^2 is low compared with the threshold of QDs emitting in blue, which is typically on the order of 1 mJ/cm^2.[15,21] In recent work[21] by Demir *et al.*, CdZnS/ZnS QDs were carefully engineered to introduce a smooth confinement potential[22,34] that causes a significant reduction of Auger rates. This engineering led to a blue ASE threshold of 60 μJ/cm^2.[21] In the case of 3CdSe NPLs, the synthesis does not involve great efforts to eliminate trap state emissions (Figures 2b and S2a). Emission quantum yield (QY) of 3CdSe NPLs is typically about 10%. Improving the emission yield of 3CdSe NPLs and their film quality will likely further reduce ASE threshold.

The modal gains of the NPL films were estimated using the variable-stripe-length (VSL) method.[35] We obtained a gain of about 600 cm^{-1} for 4CdSe and 3CdS/4CdSe/3CdS NPLs, similar to other recent reports.[17−19] These gains are a few times larger than the largest values reported for QDs and QRs.[4,36] The gains are 86 ± 7 cm^{-1} for 3CdSe and 160 ± 10 cm^{-1} for 5CdSe (Figure S3). Although the gains for 3CdSe and 5CdSe are lower, likely due to film microstructure defects or trap states, they are comparable to those of the best QDs and QRs.[4,21,36]

Nanoplatelet Lasing. We demonstrated NPL lasing using simple optical cavities between two mirrors, an output coupler and an end mirror that were parallel to each other (Figures 4a and S4). We dropcast NPLs on the output couplers to form films with thicknesses of 100 to 200 nm. The cavity lengths are typically 1 to 3 mm. Figure 4b shows pump-fluence-dependent emissions of films of 3CdSe, 4CdSe, 5CdSe, and 3CdS/4CdSe/3CdS NPLs in the cavities. Spontaneous emission is observed at low pump fluences, while sharp lasing peaks appear on the red shoulder of spontaneous emission bands at higher pump fluences. Given these long cavity lengths, the spacing between different modes is on the order of 0.1 to 0.2 nm, which cannot be resolved in our experiments with a 0.3 nm resolution. Hence, the lasing peak is a likely convolution of several lasing modes, with peak widths of 4 to 6 nm (full width at half-maximum). These lasers are similar to the operation of a typical dye laser, while they are different from single-mode or widely spaced multimode lasers using whispering-gallery-mode resonators,[10] VCSEL,[15] or self-assembled microlasers.[37] The sharp peaks in the emission spectra observed for light propagating normal to the mirror surface are evidence of lasing. The plots of pump-fluence-dependent total emission intensities indicate that the intensities increase more rapidly at fluences greater than the lasing thresholds (Figure S5).

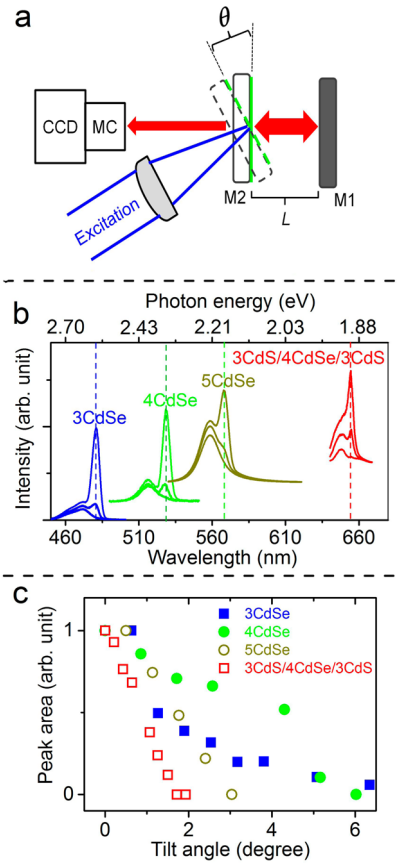

Figure 4. Red, yellow, green, and blue lasing of NPL films. (a) Scheme of lasing measurements. Arrows indicate light propagation directions. *L* is the cavity length, and θ is the cavity tilt angle. M1 is an end mirror with 100% reflectivity, and M2 is an output coupler with 90−95% reflectivity depending on wavelength. NPL films were dropcast on the surface of output coupler M2 that is facing the end mirror M1, indicated by green lines. (b) Red (3CdS/4CdSe/3CdS), yellow (5CdSe), green (4CdSe), and blue (3CdSe) lasing spectra, with the lasing peak width of ~4, ~6, ~6, and ~6 nm, respectively. Dashed lines indicate the locations of lasing peaks. For each sample, the narrow lasing peaks appear on the red side of emission at higher pump fluences. (c) Cavity-tilt-angle-dependent lasing peak area, showing the disappearance of lasing when the cavity angle was tilted.

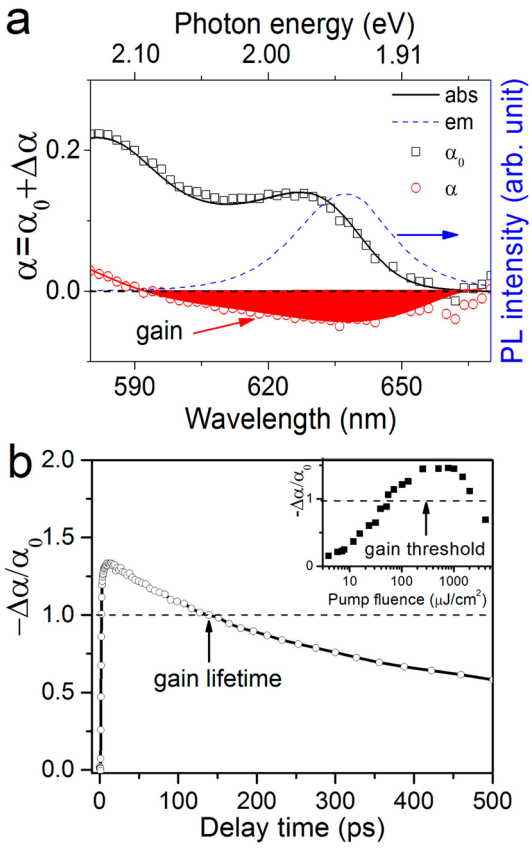

Figure 5. (a) Absorption (α_0), emission, and transient spectra (calculated as $\alpha = \alpha_0 + \Delta\alpha$) of 3CdS/4CdSe/3CdS NPLs in hexane solution. The optical gain refers to the red-shaded region where $\alpha < 0$. The excitation wavelength is 400 nm. The pump fluence was 660 μJ/cm^2, where the gain amplitude is maximized. The gain bandwidth is about 0.22 eV. (b) Dynamics of optical gain (calculated as $-\Delta\alpha/\alpha_0$) monitored at 644 nm for 3CdS/4CdSe/3CdS NPLs in hexane. Inset shows the saturation of optical gain in the region of 500−1000 μJ/cm^2. The optical gain refers to the region where $-\Delta\alpha/\alpha_0$ is greater than 1. The gain lifetime is 140 ps, where its amplitude crosses the gain threshold ($-\Delta\alpha/\alpha_0 = 1$).

Therefore, these NPL films produce red (3CdS/4CdSe/3CdS), yellow (5CdSe), green (4CdSe), and blue (3CdSe) lasing.

To confirm the lasing, we adjusted the optical cavities to manipulate the intensity of the lasing peaks. Tilting the coupler will lead to the loss of feedback and lower cavity Q factor. Since inorganic nanocrystals typically have short gain lifetimes (for QDs it is typically less than 100 ps), increasing the cavity length reduces the number of photon round trips inside the cavity before gain depletes. Indeed, the narrow-peak components in the emission spectra decreased to zero when the coupler angle was tilted by several degrees (Figure 4c) or the cavity length was increased to 1 cm (Figure S6), while the spontaneous emission remained observable (Figures S7−10).

Gain Bandwidth and Lifetime. We measured the gain bandwidth and lifetime of 3CdS/4CdSe/3CdS NPLs to provide more insights into the properties of NPLs as a gain medium. Figure 5a shows the transient spectrum (gain spectrum), calculated as $\alpha = \alpha_0 + \Delta\alpha$, of 3CdS/4CdSe/3CdS NPLs in hexane solution. The absorption spectrum (α_0) and emission spectrum are shown for comparison. Optical gain occurs in the spectral region from 595 to 655 nm (red-shaded area), where $\alpha < 0$. The same gain spectrum, calculated as $-\Delta\alpha/\alpha_0$, is also shown in Figure S11. The gain bandwidth is about 0.22 eV, which is sufficiently broad for supporting different lasing modes in practical laser applications.

Figure 5b shows the gain dynamics of 3CdS/4CdSe/3CdS in hexane monitored at 644 nm. The gain lifetime is about 140 ps, where its amplitude decays until crossing the gain threshold amplitude ($-\Delta\alpha/\alpha_0 = 1$). This lifetime is longer than those of QDs and QRs.[4,38] The inset in Figure 5b shows pump-fluence-dependent gain of solution-dispersed 3CdS/4CdSe/3CdS

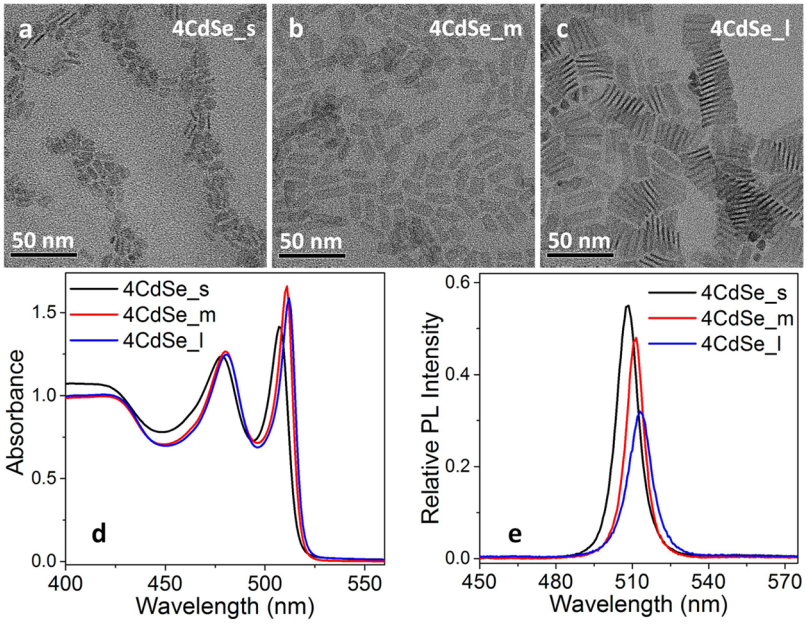

Figure 6. Transmission electron microscope images of (a) 4CdSe_s, (b) 4CdSe_m, and (c) 4CdSe_l. (d) Absorption spectra of 4CdSe_s, 4CdSe_m, and 4CdSe_l NPLs in hexane solutions. (e) Emission spectra of 4CdSe_s, 4CdSe_m, and 4CdSe_l NPLs in hexane solutions.

nanoheterostructures, which saturates above 500 μJ/cm^2. Gain decreases at pump fluences higher than 1000 μJ/cm^2, presumably because of significant Auger recombination, which reduces population inversion.[17]

NPLs with Different Lateral Dimensions. Besides the NPL thickness, the lateral dimension is another potential parameter to tune in the material design for optimization of lasing and other physical properties. To explore the role of lateral dimensions on multiexciton dynamics in CdSe NPLs, we synthesized NPLs with different lateral dimensions while keeping the NPL thickness constant. We explored the lateral dimensions within two NPL families, 4CdSe and 5CdSe. For the 4CdSe NPL family, the lateral size is tuned by controlling the reaction temperature and time. For the 5CdSe NPL family, the lateral size is tuned by varying combinations of reaction temperature, time, and precursor concentration (see Methods for details). Figure 6a−c show an example of 4CdSe NPL samples with sizes increasing from small (4CdSe_s), to medium (4CdSe_m), and to large (4CdSe_l), of which their lateral dimensions are 12 ± 2 nm by 6 ± 1 nm with corresponding NPL area 72 nm^2, 19 ± 3 nm by 7 ± 2 nm (133 nm^2 area), and 27 ± 3 nm by 8 ± 2 nm (216 nm^2), respectively. Similar tuning of lateral dimensions has been achieved for the 5CdSe NPL family (Figure S12).

For the 4CdSe NPL family, the smallest lateral dimensions slightly blue-shift the absorption and emission peaks by <5 nm when comparing 4CdSe_s and 4CdSe_l (Figure 6d,e). The peak shift is even smaller for the 5CdSe NPL family, with a <3 nm of peak shift when comparing 5CdSe_s and 5CdSe_l (Figure S12). The emission quantum yields of 4CdSe_s, 4CdSe_m, and 4CdSe_l are 55%, 48%, and 34%, respectively (Figure 6e). No significant difference in emission quantum yield (~21%) is observed for 5CdSe NPLs with different lateral dimensions. We speculate that the high PL efficiency of NPLs with smaller lateral dimensions can be explained by two effects: (i) smaller surface area of "small" NPL reduces the probability of nonradiative exciton recombination at a surface trap and (ii) NPLs with large lateral dimensions have a tendency to aggregate, forming NPL stacks that increase reabsorption and energy transfer.[30]

Effect of the NPL Lateral Dimensions on Multiexciton Dynamics and ASE. We then examined how the lateral dimension affects lasing properties including ASE threshold and gain saturation. While a lower ASE threshold helps to achieve lasing at low pump power, a high gain saturation threshold will lead to high lasing power output. We thus measured and compared ASE threshold and gain saturation of the two NPL families, 4CdSe and 5CdSe, that have different lateral dimensions. We did not notice any strong effect of lateral dimensions on the ASE threshold. Since each NPL can hold a large number of excitons,[39−41] and ASE requires only biexciton states,[19] tuning the lateral dimension in the size range in this work is not expected to affect the ASE threshold. Indeed, a recent paper by the Demir group[42] reported relatively weak dependence of the ASE threshold on the lateral dimensions of CdSe NPLs. These threshold differences are within our measurement uncertainty.

Our measurements show that the gain saturation of 5CdSe NPLs occurs at a fluence significantly higher compared to that of 4CdSe NPLs, while there is little

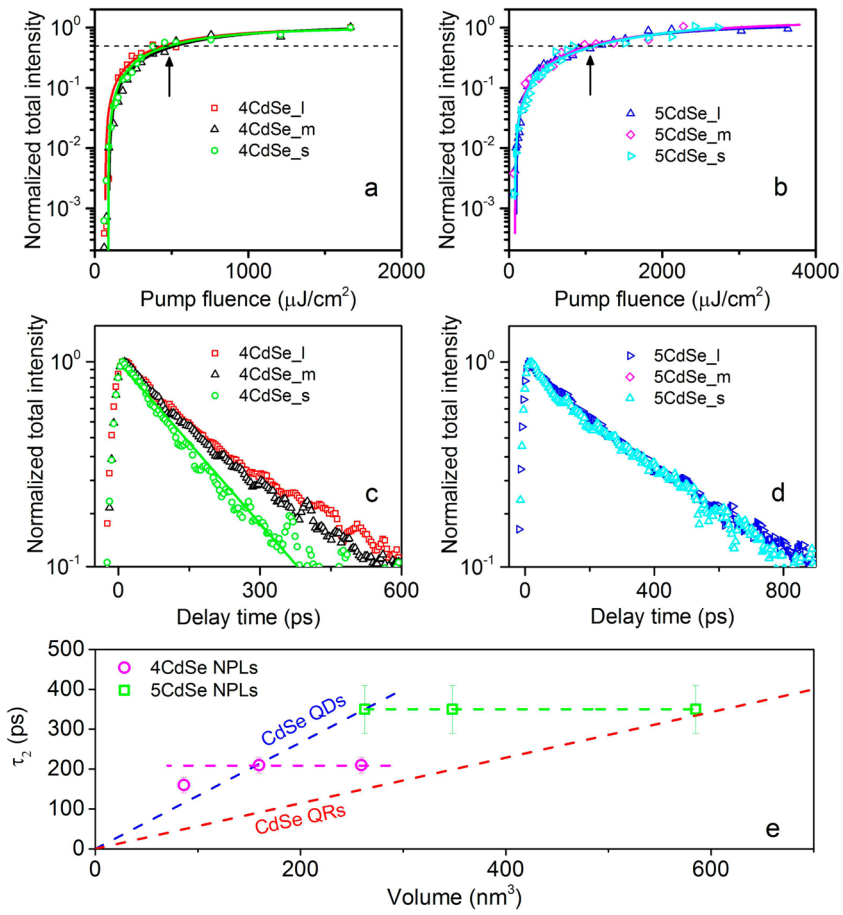

Figure 7. Normalized pump-fluence-dependent integrated ASE intensity from films of (a) 4CdSe_l, 4CdSe_m, 4CdSe_s NPLs and (b) 5CdSe_l, 5CdSe_m, 5CdSe_s NPLs. The dots are experimental data. The solid lines are fits using single-exponential rises. The arrows show the positions of saturation fluence, which is defined as the fluence at which the intensity is 50% of the saturated intensity at the plateau. No dramatic difference in the saturation fluence is observed for NPLs with the same thickness. The saturation fluence for the three 4CdSe NPLs is 500 ± 100 μJ/cm^2, and it is 1100 ± 100 μJ/cm^2 for the three 5CdSe NPLs, whose lateral dimensions are shown in Figures 6a−c and S12a−c. Auger recombination dynamics of (c) 4CdSe_l, 4CdSe_m, 4CdSe_s NPLs and (d) 5CdSe_l, 5CdSe_m, 5CdSe_s NPLs in hexane solutions. The dots are experimental data. The solid lines are fits using single-exponential decays. The lifetime is 350 ± 60 ps for 5CdSe_l, 5CdSe_m, and 5CdSe_s. It is 210 ± 20 ps for 4CdSe_l and 4CdSe_m, and 160 ± 20 ps for 4CdSe_s. The pump fluence for all the dynamics measurements is 86 μJ/cm^2. (e) Dependence of biexciton decay time (τ_2) on volume of 4CdSe and 5CdSe NPLs with different lateral dimensions. The scaling of biexciton decay time for CdSe quantum dots (QDs) and quantum rods (QRs), taken from ref 43, are shown as dashed lines for comparison.

difference for NPLs with different lateral dimensions. This comparison is indicated in Figure 7, which shows normalized pump-fluence-dependent integrated ASE intensity from 4CdSe_s, 4CdSe_m, 4CdSe_l NPLs (Figure 7a), and 5CdSe_s, 5CdSe_m, 5CdSe_l NPLs (Figure 7b). The arrows show the positions of gain saturation fluence, which is defined as the fluence at which the intensity is 50% of the saturated intensity at the plateau. The saturation fluence for 4CdSe NPLs is 500 ± 100 μJ/cm^2, and it is 1100 ± 100 μJ/cm^2 for 5CdSe NPLs.

The independence of ASE intensity of lateral dimensions in each NPL series and a higher saturation fluence in 5CdSe NPL films may be understood by examining the dynamics of multiexciton decay in CdSe NPLs. The multiexciton dynamics has been extensively studied for CdSe QDs and QRs.[43,44] It has been shown that in CdSe QDs and QRs biexciton lifetimes (τ_2) scale with the nanocrystal volume.[43] We measured Auger recombination rates for 4CdSe and 5CdSe NPL samples with different lateral dimensions using time-resolved photoluminescence spectroscopy. Since single-exciton decay times (Figure S13) are at least 1 order of magnitude longer than the lifetime of multiexciton states observed at high pump fluence (Figure S14), the Auger recombination rate can be extracted by subtracting the single-exciton decay at low fluence (0.8 μJ/cm^2) from multiexciton decay at high fluences after normalization at 1.9 ns (Figure 7c and d).[11] The analysis of the pump-fluence-dependent photoluminescence decay (Figure S15) supports the biexciton Auger recombination mechanism, in agreement with recent reports showing that carrier recombination in NPLs is generally determined by the two-exciton recombination rate.[40,41] The Auger lifetime for 4CdSe_s is 160 ± 20 ps, slightly shorter than 210 ± 20 ps measured for 4CdSe_m and 4CdSe_l NPLs (Figure 7c). Given the fact

that the volume of 4CdSe_l is 3 times larger than that of 4CdSe_s, this difference appears small compared to previous reports for CdSe QDs[11] and QRs.[38] The Auger lifetime is 350 ± 60 ps for 5CdSe_l, 5CdSe_m, and 5CdSe_s NPLs (Figure 7d) and was independent of lateral dimensions. This similarity of Auger lifetimes within each NPL family explains the lack of significant differences in gain saturation. However, the Auger lifetime is about 2 times longer in 5CdSe NPLs compared to 4CdSe NPLs. When Auger recombination competes with ASE at high fluences, gain saturation becomes more apparent. Because a longer Auger recombination lifetime helps to maintain the population of biexciton states, a higher gain saturation is expected in the 5CdSe NPL family.

We also notice a qualitative difference between biexciton dynamics in two-dimensional CdSe NPLs in comparison to both zero- and one-dimensional CdSe structures (Figure 7e). In contrast to CdSe QDs and QRs where τ_2 scales with nanocrystal volume, in CdSe NPLs τ_2 is nearly independent of lateral dimensions but strongly depends on the NPL thickness, producing a staircase-type relation between Auger rates and nanocrystal volume.

When multiple excitons are present in an NPL, their interaction can result in a biexciton state, similar to that observed in GaAs quantum wells (QWs) at cryogenic temperatures.[45] In a two-dimensional system, the binding energy of biexcitons (E_{bxx}) is expected to be about 20% of the heavy-hole/electron binding energy in a single exciton (E_{bx}), regardless of the material.[46] For CdSe NPLs surrounded by a low dielectric medium ($\varepsilon_m \approx 2$), E_{bx} was predicted to be as large as ~200 meV.[47] Thus, an estimate for E_{bxx} is ~40 meV, which is much larger than the 1−2 meV observed in epitaxially grown GaAa quantum wells,[45] but is in agreement with some experimental observations.[19] Within 200 ps following excitation with 86 μJ/cm^2 pulses, a second emission peak appeared on the red side of the band-edge emission of NPLs (Figure S16). This peak is shifted by several tens of meV from the single exciton emission and is likely to originate from the biexciton state. Moreover, the shifts between spontaneous emission and ASE peaks in Figure 3a are also close to the estimated E_{bxx} values, suggesting that ASE occurs from the biexciton state. These observations suggest the formation of the biexciton state with $E_{bxx} > k_BT$ that decays either radiatively or *via* the Auger process. For a perfect quantum well, the ratio of the Bohr radii of the biexciton and single exciton, a_{xx}/a_x, was calculated to be ~2.74, which is independent of the material.[46] It is also suggested that an exciton confined to a quantum well adopts a near-spherical shape due to an increased electron−hole Coulomb interaction.[48] As a result, the exciton volume is only a small fraction of the volume of the NPL. a_{xx} will all be smaller than the lateral dimensions of the NPL, which explains the weak dependence of the multiexciton decay rate on the NPL's lateral size (Figure 7c−e). The increase of τ_2 in 5CdSe NPLs compared to 4CdSe NPLs can be explained by the linear scaling of Auger rates with biexciton volume observed in low-dimensional CdSe and other semiconductors.[43,44] If the biexciton shape does not change much with NPL thickness, one can obtain a rough estimate of the ratio τ_2(5CdSe)/τ_2(4CdSe), which equals $(5.5/4.5)^3 \approx 1.8$. We used 5.5 and 4.5 as the thickness factors for 5CdSe and 4CdSe NPLs to account for Cd termination on either side of the NPL. This ratio is close to the experimentally observed value of 1.7 (Figure 7e). These simple arguments provide a qualitative explanation of our experimental results, although further studies will be necessary to fully rationalize the structure and dynamics of multiexcitonic states in CdSe NPLs.

CONCLUSIONS

We show that CdSe and CdS/CdSe/CdS shell/core/shell NPLs produce amplified spontaneous emission with low thresholds and high gains across the entire visible range. In particular, we show a threshold of 50 μJ/cm^2 for blue-emitting NPLs, lower than any previously reported value. We further demonstrate red, yellow, green, and blue lasing using these NPLs placed in optical cavities. For red-emitting shell/core/shell NPLs, the gain bandwidth is about 0.22 eV, sufficiently broad for practical lasing applications, and the gain lifetime is 140 ps, longer than that of QDs. Moreover, we show that the lateral dimension of the NPLs does not affect either the ASE thresholds or gain saturation levels. We also notice that multiexciton recombination in NPLs is largely independent of lateral dimensions, which is different from QDs and QRs. The higher gain saturation in 5CdSe NPLs is explained by a slower Auger recombination rate. These results suggest that this class of materials can be superior to traditional nanocrystals for lasing and optical amplification. Further work toward practical lasing devices would include understanding carrier dynamics in the NPLs and exploring ways of electrically pumping these materials.

METHODS

Synthesis. CdSe nanoplatelets were synthesized in a nitrogen environment following a previously published procedure[24] with slight modifications.

3CdSe:. In a three-neck flask, 240 mg of Cd(Ac)$_2$, 150 mL of oleic acid, and 15 mL of ODE were degassed for over 1 h at 80 °C. Then, under nitrogen flow, the flask was heated to 180 °C, and 150 mL of TOPSe at 1 M was quickly injected. The reaction was stopped after 20 min. Finally, the NPLs were washed three times with ethanol and were redispersed in hexane.

4CdSe (also termed as 4CdSe_l):. In a three-neck flask, 170 mg of Cd(myristate)$_2$, 12 mg of Se, and 15 mL of ODE were degassed

for 1 h at room temperature. Then, under nitrogen flow, the flask was heated rapidly to 240 °C. When the temperature reached 190 °C, 40 mg of $Cd(Ac)_2$ was quickly introduced. The solution was held at 240 °C for 5 min, and the reaction was then stopped. The temperature was reduced to 70 °C, and 2 mL of oleic acid and 15 mL of hexane were added. The mixture was then centrifuged, and the precipitate containing the NPLs was resuspended in hexane.

4CdSe_m:. The synthesis procedure is the same as that for 4CdSe, except that the reaction was kept at 240 °C for 1 min instead of 5 min.

4CdSe_s:. The synthesis procedure is the same as that for 4CdSe, except that the reaction was stopped at 225 °C before reaching 240 °C after introducing 40 mg of $Cd(Ac)_2$.

5CdSe (also termed as 5CdSe_s):. In a three-neck flask, 170 mg of $Cd(myristate)_2$ and 14 mL of octadecene (ODE) were degassed for 30 min at room temperature. Then, under nitrogen flow, the flask was heated to 240 °C and 1 mL of a 0.15 M solution of selenium powder sonicated in ODE was injected. After 20 s of reaction, 60 mg of $Cd(Ac)_2$ was introduced. The solution was held at 240 °C for 10 min, and the temperature was then rapidly reduced to stop the reaction. A 2 mL amount of oleic acid and 15 mL of hexane were added. The mixture was then centrifuged, and the precipitate containing the NPLs was resuspended in hexane.

5CdSe_l:. In a three-neck flask, 170 mg of $Cd(myristate)_2$ in 13.5 mL of ODE was degassed at room temperature. Under nitrogen flow, the flask was heated to 250 °C, and then 12 mg of Se powder predispersed in 1.5 mL of 0.1 M Se-ODE was injected into the solution. A 120 mg portion of finely ground $Cd(OAc)_2$ was then introduced after 60 s. The reaction was then kept for 10 min. Then 2 mL of oleic acid in 15 mL of ODE was injected, when the reaction was cooled to 100 °C.

5CdSe_m:. The procedure is similar to that of 5CdSe except that 90 mg of $Cd(OAc)_2$ was used and that the reaction was kept at 245 °C for 10 min.

3CdS/4CdSe/3CdS:. These shell/core/shell NPLs were synthesized following one of the variants of the colloidal atomic layer deposition approach[25] with some modifications and optimizations. Before shell growth, 4CdSe NPLs, synthesized as described above, were redispersed in hexane three times to remove free Cd^{2+} in the solution. Then, the first layer of S^{2-} was introduced by phase transferring 4CdSe NPLs from hexane to 5 mL of *N*-methylformamide (NMF), in which 50 μL of aqueous solution of ammonium sulfide (40%) was dissolved. After phase separation, acetonitrile and toluene were added to precipitate the NPLs, and they were then dispersed in 5 mL of NMF. To grow the first layer of Cd, we redispersed the solution in 2 mL of NMF, introduced 2.5 mL of 0.2 M cadmium acetate in NMF, and stirred the solution for 1 min. Then, we precipitated the NPLs with toluene, centrifuged them, and redispersed the precipitate in 5 mL of NMF. The first monolayer of CdS shell growth was completed at this stage, with the surfaces terminated by Cd layers. To grow a thickness of x monolayers of CdS, the above steps were repeated x times. The final shell/core/shell NPLs were dispersed in 5 mL of hexane with the addition of 250 μL of dried 70% technical-grade oleylamine.

Film Deposition. We first precipitated the NPLs from the above solution using ethanol to remove excess oleylamine. We then redispersed the NPLs in 1 mL of a 4:1 (v/v) hexane/octane mixture and filtered the solution through a membrane filter. The resulting solution was then spin coated on a glass substrate for ASE measurements. For the measurements of refractive index, the NPLs were spin coated on silicon substrates. For lasing demonstration, NPLs were dropcast on partial reflective mirrors (output couplers).

Electron Microscope Imaging. TEM images were obtained using a 300 kV FEI Tecnai F30 microscope.

Absorption and emission. Absorption and emission spectra were collected on a Cary 5000 spectrometer (Agilent) and a Nanolog fluorometer (Horiba JY), respectively.

Film Properties. The refractive indices (n_{sample}) of the NPL films were measured using an ellipsometer (Gaertner Scientific LSE-WS, wavelength of 632 nm for CdSe NPL films; Horiba Jobin Yvon UVISEL, wavelength of 650 nm for 3CdS/4CdSe/3CdS NPL films). Average values were determined over areas 10 mm in diameter. From these values, the packing density was calculated according to $D = (n_{sample} - n_{air})/(n_{CdSe} - n_{air})$, with n_{air} taken to be 1 and n_{CdSe} taken to be 2.4.

Amplified Spontaneous Emission. The films were excited with 400 nm pulses obtained by frequency doubling the Ti:sapphire amplifier output. The laser beam was focused onto a stripe along the NPL films using a cylindrical lens. The width of the stripe, defined as the width that contains 60% of the power in the laser beam, was determined using the knife-edge technique. In a typical ASE experiment, the stripe was 2 mm in length and 60 μm in width. The emission was measured from the edge of the films along the direction of the strip, and it is perpendicular to the propagation direction of the incident pump beam. All measurements were made at room temperature in air. Two different excitation−detection systems were employed in this work. In the first system, the excitation was provided by an amplified Ti:sapphire laser system (Spectra-Physics Spitfire Pro, 35 fs, 800 nm, 100 Hz), and the emission was collected by a grating spectrometer (Acton SP2300, Princeton Instruments) coupled with a charge-coupled device (CCD) detector. In the second system, the excitation was provided by an amplified Ti:sapphire laser system (Legend, Coherent Inc., 35 fs, 800 nm, 100 Hz), and the emission was detected using a USB spectrometer (QE Pro, Ocean Optics). Consistent results were obtained using these two systems.

In the gain saturation measurement, the films were covered by another glass slide to minimize sample exposure to air under high pump fluence. The films were also constantly moved during the measurements to ensure that ASE spectra came from undamaged areas on samples.

In a variable stripe length measurement of emission and ASE, the stripe width is fixed while the length is controlled by blocking a portion of the laser beam using a razor blade mounted on a micrometer. The maximum stripe length is less than 2 mm and is located near the center of a laser beam (>5 mm in diameter) to achieve uniform illumination.

Lasing in Optical Cavities. The typical optical cavity consisted of two mirrors aligned in parallel. One is a partial reflective mirror (CVI Laser Optics, 90−95% reflectivity depending on wavelength), and the other is a silver mirror (Thorlabs, 100% reflectivity). The angle of output coupler is adjustable. The end mirror is placed on a translation stage. The films were dropcast on the output couplers without pretreating the coupler coatings because the identity of the reflective coatings is unknown. Consequently, NPL films on the output couplers were not uniform. The excitation pulses (400 nm, 100 Hz) were gently focused onto the films from the back side of the couplers (15° from the normal). The emission collected from the normal was sent to the first detection system mentioned above. Reflection from the back side of the output couplers and scattering from nonuniform films caused losses of excitation pump power. In each of the three spectra in Figure 4b, from low to high intensities, the pump fluences are 254, 306, and 408 $\mu J/cm^2$ for 3CdSe, 153, 174, and 245 $\mu J/cm^2$ for 4CdSe, 254, 326, and 438 $\mu J/cm^2$ for 5CdSe, and 217, 334, and 427 $\mu J/cm^2$ for 3CdS/4CdSe/3CdS, respectively. The fluences have been corrected to exclude the reflection loss by the output coupler.

Gain Bandwidth and Dynamics. A single-channel Si detector was used to measure the absorption (α_0) and transient absorption ($\Delta\alpha$) at each wavelength. The gain spectrum (α) was then calculated as $\alpha = \alpha_0 + \Delta\alpha$ at each wavelength. The gain dynamics ($\Delta\alpha/\alpha_0$, maximum at 644 nm) was measured at 660 $\mu J/cm^2$.

Time-Resolved Photoluminescence Measurements. Excitation of the films is provided by frequency doubling the output of an amplified Ti:sapphire laser system (Spectra-Physics Spitfire Pro). The pulses have a wavelength of 400 nm, a duration of approximately 35 fs, and a repetition rate of 2000 Hz. We resolved PL as a function of wavelength and time after excitation using a streak camera (Hamamatsu C5680) with photon-counting detection.

Conflict of Interest: The authors declare no competing financial interest.

Acknowledgment. This work was supported by the Air Force Office of Scientific Research under grant number FA9550-14-1-0367, by the University of Chicago NSF MRSEC Program under Award Number DMR-14-20703, and by the II–VI Foundation. Use of the Center for Nanoscale Materials was supported by the U.S. Department of Energy, Office of Science, Office of Basic Energy Sciences, under Contract No. DE-AC02-06CH11357. P.D.D. acknowledges support from the NSF GRFP and from the Graduate Program in Biophysical Sciences at the University of Chicago (NIH Grant T32 Eb009412).

Supporting Information Available: The Supporting Information is available free of charge on the ACS Publications website at DOI: 10.1021/acsnano.5b02509.

PL excitation spectra, pump-fluence-dependent lasing intensities, lasing spectra from adjusted optical cavities, and analysis of Auger recombination rates (PDF)

REFERENCES AND NOTES

1. Talapin, D. V.; Lee, J. S.; Kovalenko, M. V.; Shevchenko, E. V. Prospects of Colloidal Nanocrystals for Electronic and Optoelectronic Applications. *Chem. Rev.* **2010**, *110*, 389–458.
2. Klimov, V. I.; Mikhailovsky, A. A.; Xu, S.; Malko, A.; Hollingsworth, J. A.; Leatherdale, C. A.; Eisler, H. J.; Bawendi, M. G. Optical Gain and Stimulated Emission in Nanocrystal Quantum Dots. *Science* **2000**, *290*, 314–317.
3. Eisler, H. J.; Sundar, V. C.; Bawendi, M. G.; Walsh, M.; Smith, H. I.; Klimov, V. Color-Selective Semiconductor Nanocrystal Laser. *Appl. Phys. Lett.* **2002**, *80*, 4614–4616.
4. Malko, A. V.; Mikhailovsky, A. A.; Petruska, M. A.; Hollingsworth, J. A.; Htoon, H.; Bawendi, M. G.; Klimov, V. I. From Amplified Spontaneous Emission to Microring Lasing Using Nanocrystal Quantum Dot Solids. *Appl. Phys. Lett.* **2002**, *81*, 1303–1305.
5. Kazes, M.; Lewis, D. Y.; Ebenstein, Y.; Mokari, T.; Banin, U. Lasing From Semiconductor Quantum Rods in a Cylindrical Microcavity. *Adv. Mater.* **2002**, *14*, 317–321.
6. Caruge, J. M.; Chan, Y. T.; Sundar, V.; Eisler, H. J.; Bawendi, M. G. Transient Photoluminescence and Simultaneous Amplified Spontaneous Emission From Multiexciton States in CdSe Quantum Dots. *Phys. Rev. B: Condens. Matter Mater. Phys.* **2004**, *70*, 085316.
7. Ivanov, S. A.; Nanda, J.; Piryatinski, A.; Achermann, M.; Balet, L. P.; Bezel, I. V.; Anikeeva, P. O.; Tretiak, S.; Klimov, V. I. Light Amplification Using Inverted Core/Shell Nanocrystals: Towards Lasing in the Single-Exciton Regime. *J. Phys. Chem. B* **2004**, *108*, 10625–10630.
8. Klimov, V. I.; Ivanov, S. A.; Nanda, J.; Achermann, M.; Bezel, I.; McGuire, J. A.; Piryatinski, A. Single-Exciton Optical Gain in Semiconductor Nanocrystals. *Nature* **2007**, *447*, 441–446.
9. Zavelani-Rossi, M.; Lupo, M. G.; Krahne, R.; Manna, L.; Lanzani, G. Lasing in Self-Assembled Microcavities of CdSe/CdS Core/Shell Colloidal Quantum Rods. *Nanoscale* **2010**, *2*, 931–935.
10. Grivas, C.; Li, C. Y.; Andreakou, P.; Wang, P. F.; Ding, M.; Brambilla, G.; Manna, L.; Lagoudakis, P. Single-Mode Tunable Laser Emission in the Single-Exciton Regime From Colloidal Nanocrystals. *Nat. Commun.* **2013**, *4*, 2376.
11. Klimov, V. I.; Mikhailovsky, A. A.; McBranch, D. W.; Leatherdale, C. A.; Bawendi, M. G. Quantization of Multiparticle Auger Rates in Semiconductor Quantum Dots. *Science* **2000**, *287*, 1011–1013.
12. Garcia-Santamaria, F.; Chen, Y. F.; Vela, J.; Schaller, R. D.; Hollingsworth, J. A.; Klimov, V. I. Suppressed Auger Recombination in "Giant" Nanocrystals Boosts Optical Gain Performance. *Nano Lett.* **2009**, *9*, 3482–3488.
13. Liao, Y. L.; Xing, G. C.; Mishra, N.; Sum, T. C.; Chan, Y. Low Threshold, Amplified Spontaneous Emission from Core-Seeded Semiconductor Nanotetrapods Incorporated into a Sol-Gel Matrix. *Adv. Mater.* **2012**, *24*, Op159–Op164.
14. Wang, C. J.; Wehrenberg, B. L.; Woo, C. Y.; Guyot-Sionnest, P. Light Emission and Amplification in Charged CdSe Quantum Dots. *J. Phys. Chem. B* **2004**, *108*, 9027–9031.
15. Dang, C.; Lee, J.; Breen, C.; Steckel, J. S.; Coe-Sullivan, S.; Nurmikko, A. Red, Green and Blue Lasing Enabled by Single-Exciton Gain in Colloidal Quantum Dot Films. *Nat. Nanotechnol.* **2012**, *7*, 335–339.
16. Ithurria, S.; Tessier, M. D.; Mahler, B.; Lobo, R. P. S. M.; Dubertret, B.; Efros, A. Colloidal Nanoplatelets With Two-Dimensional Electronic Structure. *Nat. Mater.* **2011**, *10*, 936–941.
17. She, C. X.; Fedin, I.; Dolzhnikov, D. S.; Demortière, A.; Schaller, R. D.; Pelton, M.; Talapin, D. V. Low-Threshold Stimulated Emission Using Colloidal Quantum Wells. *Nano Lett.* **2014**, *14*, 2772–2777.
18. Guzelturk, B.; Kelestemur, Y.; Olutas, M.; Delikanli, S.; Demir, H. V. Amplified Spontaneous Emission and Lasing in Colloidal Nanoplatelets. *ACS Nano* **2014**, *8*, 6599–6605.
19. Grim, J. Q.; Christodoulou, S.; Di Stasio, F.; Krahne, R.; Cingolani, R.; Manna, L.; Moreels, I. Continuous-Wave Biexciton Lasing at Room Temperature Using Solution-Processed Quantum Wells. *Nat. Nanotechnol.* **2014**, *9*, 891–895.
20. Chan, Y.; Steckel, J. S.; Snee, P. T.; Caruge, J. M.; Hodgkiss, J. M.; Nocera, D. G.; Bawendi, M. G. Blue semiconductor nanocrystal laser. *Appl. Phys. Lett.* **2005**, *86*, 073102.
21. Guzelturk, B.; Kelestemur, Y.; Akgul, M. Z.; Sharma, V. K.; Demir, H. V. Ultralow Threshold One-Photon- and Two-Photon-Pumped Optical Gain Media of Blue-Emitting Colloidal Quantum Dot Films. *J. Phys. Chem. Lett.* **2014**, *5*, 2214–2218.
22. Wang, X. Y.; Ren, X. F.; Kahen, K.; Hahn, M. A.; Rajeswaran, M.; Maccagnano-Zacher, S.; Silcox, J.; Cragg, G. E.; Efros, A. L.; Krauss, T. D. Non-blinking semiconductor nanocrystals. *Nature* **2009**, *459*, 686–689.
23. Chan, Y.; Caruge, J. M.; Snee, P. T.; Bawendi, M. G. Multiexcitonic two-state lasing in a CdSe nanocrystal laser. *Appl. Phys. Lett.* **2004**, *85*, 2460–2462.
24. Ithurria, S.; Bousquet, G.; Dubertret, B. Continuous Transition from 3D to 1D Confinement Observed during the Formation of CdSe Nanoplatelets. *J. Am. Chem. Soc.* **2011**, *133*, 3070–3077.
25. Ithurria, S.; Talapin, D. V. Colloidal Atomic Layer Deposition (c-ALD) using Self-Limiting Reactions at Nanocrystal Surface Coupled to Phase Transfer between Polar and Nonpolar Media. *J. Am. Chem. Soc.* **2012**, *134*, 18585–18590.
26. Ithurria, S.; Dubertret, B. Quasi 2D Colloidal CdSe Platelets with Thicknesses Controlled at the Atomic Level. *J. Am. Chem. Soc.* **2008**, *130*, 16504–16506.
27. Tessier, M. D.; Javaux, C.; Maksimovic, I.; Loriette, V.; Dubertret, B. Spectroscopy of Single CdSe Nanoplatelets. *ACS Nano* **2012**, *6*, 6751–6758.
28. Mahler, B.; Nadal, B.; Bouet, C.; Patriarche, G.; Dubertret, B. Core/Shell Colloidal Semiconductor Nanoplatelets. *J. Am. Chem. Soc.* **2012**, *134*, 18591–18598.
29. Tessier, M. D.; Mahler, B.; Nadal, B.; Heuclin, H.; Pedetti, S.; Dubertret, B. Spectroscopy of Colloidal Semiconductor Core/Shell Nanoplatelets With High Quantum Yield. *Nano Lett.* **2013**, *13*, 3321–3328.
30. Rowland, C. E.; Fedin, I.; Zhang, H.; Gray, S. K.; Govorov, A. O.; Talapin, D. V.; Schaller, R. D. Picosecond Energy Transfer and Multiexciton Transfer Outpaces Auger Recombination in Binary CdSe Nanoplatelet Solids. *Nat. Mater.* **2015**, *14*, 484–489.
31. Kagan, C. R.; Murray, C. B.; Bawendi, M. G. Long-Range Resonance Transfer of Electronic Excitations in Close-Packed CdSe Quantum-Dot Solids. *Phys. Rev. B: Condens. Matter Mater. Phys.* **1996**, *54*, 8633–8643.
32. Guzelturk, B.; Erdem, O.; Olutas, M.; Kelestemur, Y.; Demir, H. V. Stacking in Colloidal Nanoplatelets: Tuning Excitonic Properties. *ACS Nano* **2014**, *8*, 12524–12533.
33. Sholin, V.; Olson, J. D.; Carter, S. A. Semiconducting Polymers and Quantum Dots in Luminescent Solar Concentrators for Solar Energy Harvesting. *J. Appl. Phys.* **2007**, *101*, 123114.
34. Cragg, G. E.; Efros, A. L. Suppression of Auger Processes in Confined Structures. *Nano Lett.* **2010**, *10*, 313–317.

35. Shaklee, K. L.; Leheny, R. F. Direct Determination of Optical Gain in Semiconductor Crystals. *Appl. Phys. Lett.* **1971**, *18*, 475–477.
36. Kazes, M.; Oron, D.; Shweky, I.; Banin, U. Temperature Dependence of Optical Gain in CdSe/ZnS Quantum Rods. *J. Phys. Chem. C* **2007**, *111*, 7898–7905.
37. Di Stasio, F.; Grim, J. Q.; Lesnyak, V.; Rastogi, P.; Manna, L.; Moreels, I.; Krahne, R. Single-Mode Lasing from Colloidal Water-Soluble CdSe/CdS Quantum Dot-in-Rods. *Small* **2015**, *11*, 1328–1334.
38. Htoon, H.; Hollingworth, J. A.; Malko, A. V.; Dickerson, R.; Klimov, V. I. Light Amplification in Semiconductor Nanocrystals: Quantum Rods *versus* Quantum Dots. *Appl. Phys. Lett.* **2003**, *82*, 4776–4778.
39. Pelton, M.; Ithurria, S.; Schaller, R. D.; Dolzhnikov, D. S.; Talapin, D. V. Carrier Cooling in Colloidal Quantum Wells. *Nano Lett.* **2012**, *12*, 6158–6163.
40. Baghani, E.; O'Leary, S. K.; Fedin, I.; Talapin, D. V.; Pelton, M. Auger-Limited Carrier Recombination and Relaxation in CdSe Colloidal Quantum Wells. *J. Phys. Chem. Lett.* **2015**, *6*, 1032–1036.
41. Kunneman, L. T.; Tessier, M. D.; Heuclin, H.; Dubertret, B.; Aulin, Y. V.; Grozema, F. C.; Schins, J. M.; Siebbeles, L. D. A. Bimolecular Auger Recombination of Electron−Hole Pairs in Two-Dimensional CdSe and CdSe/CdZnS Core/Shell Nanoplatelets. *J. Phys. Chem. Lett.* **2013**, *4*, 3574–3578.
42. Olutas, M.; Guzelturk, B.; Kelestemur, Y.; Yeltik, A.; Delikanli, S.; Demir, H. V. Lateral Size-Dependent Spontaneous and Stimulated Emission Properties in Colloidal CdSe Nanoplatelets. *ACS Nano* **2015**, *9*, 5041–5050.
43. Htoon, H.; Hollingsworth, J. A.; Dickerson, R.; Klimov, V. I. Effect of Zero- to One-Dimensional Transformation on Multiparticle Auger Recombination in Semiconductor Quantum Rods. *Phys. Rev. Lett.* **2003**, *91*, 227401.
44. Klimov, V. I.; McGuire, J. A.; Schaller, R. D.; Rupasov, V. I. Scaling of Multiexciton Lifetimes in Semiconductor Nanocrystals. *Phys. Rev. B: Condens. Matter Mater. Phys.* **2008**, *77*, 195324.
45. Birkedal, D.; Singh, J.; Lyssenko, V. G.; Erland, J.; Hvam, J. M. Binding of Quasi-Two-Dimensional Biexcitons. *Phys. Rev. Lett.* **1996**, *76*, 672–675.
46. Singh, J.; Birkedal, D.; Lyssenko, V. G.; Hvam, J. M. Binding Energy of Two-Dimensional Biexcitons. *Phys. Rev. B: Condens. Matter Mater. Phys.* **1996**, *53*, 15909–15913.
47. Achtstein, A. W.; Schliwa, A.; Prudnikau, A.; Hardzei, M.; Artemyev, M. V.; Thomsen, C.; Woggon, U. Electronic Structure and Exciton−Phonon Interaction in Two-Dimensional Colloidal CdSe Nanosheets. *Nano Lett.* **2012**, *12*, 3151–3157.
48. Miller, D. A. B. Optical Physics of Quantum Wells. In *Quantum Dynamics of Simple Systems*, Oppo, G. -L.; Barnett, S. M.; Riis, E.; Wilkinson, M., Eds.; Institute of Physics: London, 1996; pp 239−266.